[Peter Kutne, Bhavin K. Kapadia, Wolfgang Meier, Manfred Aigner, Experimental Analysis of the Combustion Behaviour of Oxyfuel Flames in a Gas Turbine Model Combustor, Proceedings of the Combustion Institute, Volume 33, Issue 2, 2011, pages 3383-3390.]

The original publication is available at www.elsevier.com

http://dx.doi.org/doi:10.1016/j.proci.2010.07.008

Experimental Analysis of the Combustion Behaviour of Oxyfuel Flames in a Gas Turbine Model Combustor

Peter Kutne*, Bhavin K. Kapadia, Wolfgang Meier, Manfred Aigner

Deutsches Zentrum für Luft- und Raumfahrt (DLR), Institut für Verbrennungstechnik, Pfaffenwaldring 38, D-70569 Stuttgart, Germany

Abstract

Power generation by using oxyfuel combustion in a gas turbine cycle is a promising option to reduce carbon dioxide (CO_2) emission, while using fossil fuels. In order to use this process some significant changes to the gas turbine are required, regarding which open questions still exist. An important question is whether reliable operation with oxyfuel combustion under gas turbine conditions is possible. The paper describes experiments on partially-premixed swirl stabilized oxyfuel flames carried out in a gas turbine model combustor at atmospheric pressure. To characterize the behaviour of the oxyfuel flames a systematic parameter study for oxidisers consisting of 20 % - 40 % oxygen (O_2), equivalence ratios from 0.5 to 1, and powers of 10 kW to 30 kW was carried out. OH^*-chemiluminescence imaging was used to visualise the flame structure and stability. The results show a strong influence of the O_2 concentration on the combustion behavior in contrast to the equivalence ratio which has only a very small effect. To obtain quantitative results, laser Raman scattering has been used on selected flames to measure simulta-

*Corresponding author. Fax: +49 711 6862578, Email: peter.kutne@dlr.de

neously the major species concentrations, mixture fraction and temperature. The results reveal differences in the flame stabilisation mechanism, compared to methane (CH_4)/air flames in the same burner.
Keywords: Oxyfuel combustion, gas turbine model combustor, laser Raman scattering

1. Introduction

The reduction of CO_2 emissions has become a major topic of research in the last decade due to the negative environmental impact of CO_2 and other green house gases on world climate. In 2007 the European Commission has declared to reduce the emission of greenhouse gases by 20 % until 2020 and increase the use of renewable energy. Though there are big efforts in the area of renewable energy sources, the fossil fuels will remain the largest source for energy conversion in the next decades. Thus there is an increased interest in power generation industry towards technologies, which help to reduce CO_2 emissions from fossil fuels. These technologies can encompass either upgradation of existing power plants or use of new systems which can provide a significant advantage. This interest of industry is documented by a large number of EU projects with industrial involvement, the likes of ENCAP, DECARBit, BIGCCS, CAESAR, CACHET, DYNAMIS, CAPRICE, COACH, ECCO, NANOGLOWA, CLC Gas Power. The importance of CO_2 capture technologies for the reduction of CO_2 emissions is also approved by a study of McKinsey ("Carbon Capture & Storage: Assessing the economics") [1], presented at the EC in Bruessel in 2008.

The oxyfuel combustion of coal in a steam turbine process is regarded

as a possible way to use the oxyfuel process for CO_2 reduction. Research on this field is very active with the outcome that the first demonstration plants are in operation, and the power generation industry is willing to invest in this technology. Another way of particular interest is the use of oxyfuel combustion in gas turbines. This process offers the possibility to use the same post combustion techniques as for the oxyfuel coal process, in combination with an efficient combined cycle process. The Graz cycle introduced in 1995 by Jericha et al. [2] is such a cycle that continues to be improved [3, 4, 5]. Despite the general interest in the process, the oxyfuel combustion for gas turbines has never been taken beyond thermodynamic calculations. Initially the large effort due to the air separation unit (ASU) is seen as one reason, as for this form of combustion part of the turbine energy is used by the ASU to remove the N_2 present in air. In the meanwhile there has been a considerable development of ASUs, in particular as parts of a power plant. There are also several oxyfuel processes promising high efficiency that offset the energy loss due to the air separation making this process competitive to other CO_2 avoiding techniques. The crux of the matter seems to be the changes in the turbo machinery that must accompany changes in the burner. Since this process replaces nitrogen (N_2) by CO_2 and hence uses a mixture of steam and CO_2 as a working fluid, the turbo machinery has to be adapted to the different physical properties. At high flame temperatures CO_2 has a heat capacity more than 1.6 times higher as that of N_2. Because CO_2 is an infrared active molecule the radiant heat transfer has to be taken into account. Beside the physical differences the high amount of CO_2 has also an effect on the chemical reactions, because it can act as a reaction partner

and its high chaperon efficiency enhances third body reactions. In addition the cycle calculations indicate, that a gas turbine for oxyfuel combustion has to work at higher pressures than existing stationary gas turbines. Assuming that it is feasible to build such a turbine, another question arises: Is the oxyfuel combustion under gas turbine conditions viable?

Williams et al. [6] investigated syngas and methane flames for premixed swirl stabilised conditions for two different oxidisers of air and $O_2/CO_2/N_2$. Simple flame images for different conditions have been presented along with exhaust gas emissions. They report lower nitrogen oxides concentrations (NO_x) for the quasi-oxyfuel flames and higher carbon monoxide concentrations (CO), suggesting stoichiometric operation at 20-24% O_2 as ideal for low emissions. Sautet et al. [7] studied the length of natural gas/oxygen diffusion flames in a jet burner for free and confined configurations. Fuel jet Reynolds numbers were varied from 8362-16300 for 5 flames of which two were buoyancy controlled. The flame lengths were calculated from OH^*-chemiluminescence and indicated flames to be 2-3 times shorter than air flames with adiabatic flame temperatures in the region of 3050 K. Ditaranto and Hals [8] discussed the effect of stoichiometric operation and high O_2 content in oxidiser on thermo-acoustic oscillations in sudden expansion jet configuration. They reported occurrence of thermo-acoustic instabilities as O_2 content in the oxidiser was increased, characterising different instability modes dependant on flow velocity and flame speed variations. Open questions still exist regarding flame characteristics when oxyfuel mixtures substitute conventional air operation in a gas turbine burner. Aspects pertaining to the kind of flame suitable, i.e., diffusion/premixed/partially premixed, the

optimum CO_2 dilution in oxidiser for stable operation, consequent exhaust gas temperatures, and occurrence of instabilities in the combustor need to be addressed. The work presented here seeks to answer some of these questions by investigating atmospheric pressure flames on a technical swirl combustor. The combustor is fuelled with CH_4 and a mixture of CO_2 and O_2 as oxidiser. Two sets of experiments were conducted with the first focusing on determining flame stability for equivalence ratios 0.5 to 1, and for different O_2 concentrations in oxidiser. OH^*-chemiluminescence imaging is used to visualize the size, shape and position of heat release zone. The second set of experiments involve laser Raman scattering measurements to characterize the flames in detail by obtaining the main species concentration, mixture fraction and temperature, which would also serve as a database for model validation. For the purpose of comparison with earlier measurements of CH_4/air flames, lean operation conditions were chosen for the Raman measurements, although stoichiometric conditions would be more relevant for technical application of oxyfuel combustion. Investigation of technical operation condition, with pressurized flames, preheated oxidiser and stoichiometric conditions will be the focus of measurements planned in 2010.

2. Experimental setup

2.1. Burner Geometry

The burner used was a gas turbine model combustor (DLR dual swirl burner), as shown in Fig. 1. The burner design originates from a gas turbine combustor with an air blast nozzle for liquid fuels, which is modified for gaseous fuel operation. This burner configuration was used in several projects

before for CH_4/air combustion under atmospheric and high pressure (detailed description of the burner[9]). So a detailed data base exists to compare the oxyfuel flames to normal air combustion [9].

The oxidiser mixture was supplied through a central nozzle (diameter 15 mm) and an annular nozzle (i.d. 17 mm, o.d. 25 mm contoured to an o.d. of 40 mm) as a co-swirling flow to the flame. Between the two oxidiser flows the CH_4 was fed through a ring of 72 channels (0.5 mm x 0.5 mm). The exit plane of the fuel inlet and the inner oxidiser nozzle is located 4.5 mm below the exit plane of the outer air nozzle. The overall flow field of the flames is characterised by a conically shaped inflow of fresh gas, an inner recirculation zone (IRZ) and outer recirculation zone (ORZ) as sketched in Fig. 1. In the shear layer formed between the inflow and the IRZ, the mixing of hot combustion products with fresh gas leads to a continuous ignition and stabilization of the flame. The burner was mounted in an optically accessible combustion chamber. The chamber measures 85 x 85 mm (cross-section) and is 120 mm height. It consists of four planar quartz windows supported at the corners by steel posts (diameter 10 mm). The flow exits the chamber through a rectangular to conical exhaust section. All gas flows are controlled via mass flow controllers, which where calibrated in house. The O_2 and CO_2 are premixed upstream of the combustor plenum by a mixing unit (Sulzer, type SMI-W).

2.2. OH-Chemiluminescence Imaging*

OH^* (electronically excited) chemiluminescence was used to study the size and shape of the heat release zone. The OH^* chemiluminescence detection system consisted of an image-intensified CCD camera (Roper Scientific, 512

x 512 pixels) with achromatic UV lens (Halle, f = 100 mm). OH^* chemiluminescence near 310 nm was detected through an interference filter in the wavelength region 295-340 nm. The exposure time for the image intensifier was set to 400 μs to capture the integrated (along the line of sight) spontaneous emission from OH in the electronically excited state (OH^*). For each measurement point 200 images were recorded.

OH^* chemiluminescence signals are line-of-sight integrated and thus the spatial resolution is compromised. Moreover, the exact effects of strain rate and the gas composition on the OH^* concentrations are not known in detail, especially for such high CO_2 concentrations. For that reason, it is not possible to interpret the chemiluminescence images quantitatively. Nonetheless, OH^* chemiluminescence signals are a qualitative marker for the regions of high heat release and therefore a good indicator of the position and shape of the flame zone.

2.3. Laser Raman Scattering

Laser Raman scattering was applied to measure the major species concentration, mixture fraction, and temperature simultaneously. The setup consists of 3 double-pulse Nd:YAG laser systems, a pulse stretcher, a focussing lens, the detection optics, a spectrograph, and an ICCD camera. The 3 Nd:YAG lasers (Spectra-Physics PIV 400) provide 6 pulses at λ=532 nm of 7 ns duration each at a repetition rate of 10 Hz which are combined to one beam. To reduce the intensity at the windows and to avoid optical breakdown in the focal region the pulses were elongated by a pulse stretcher, and furthermore the laser beams were focused by a combination of two perpendicularly arranged cylindrical lenses (f = 300 mm) to generate a blurred focus

of an average diameter $\leq$0.5 mm. In this way, a total pulse energy of 0.9 J could be irradiated into the combustor. The pulse stretcher consists of two beam splitters and six mirrors, which divide each pulse into a number of individual pulses. After travelling along different path ways, the individual pulses are re-combined yielding a pulse with duration of about 350 ns [11]. The Raman scattered light was collected at 90° by an achromatic lens system with an aperture of 150 mm and relayed onto the entrance slit of the spectrograph (SpectraPro 300i, Acton Research, f=300 mm, 490 lines/mm, f#=4, dispersion 6 nm/mm). For rejection of elastically scattered light a holographic notch filter was placed in front of the entrance slit. A slit width of 1 mm, a slit height of 14 mm and a magnification of the detection optics of 2 resulted in an imaged probe volume of 7 mm in direction of the laser beam and 0.5 mm in diameter. After spectral separation, the Raman bands from the different molecular species (CO_2, O_2, CO, N_2, CH_4, H_2O, and H_2) were detected by an intensified CCD camera (1340 x 1300 pixels) along the line of 7 mm. The images were binned on chip to super pixels (268 points on the spectral axis and 28 on the spatial axis). This yielded 28 measurement volumes of 0.25 mm length each. The sampling rate of the ICCD is 10 Hz and the gate time used was 1 μs. The energy of the total beam recorded by a power meter before the measurement volume was used for normalization of the measured Raman signals. Due to the presence of carbon atoms in the oxidiser and in the fuel, it was not possible to define a mixture fraction by using carbon-containing species. Therefore the mixture fraction was derived from hydrogen-based species. To determine the mixture fraction the concentration of all hydrogen containing species (methane, water and hydrogen)

were used to calculate the element mole fraction of hydrogen Z_{H_2} with formula 1. The coefficient $\mu_{H,Y}$ denotes the molar proportion of hydrogen in species Y. The coefficient X_Y is the mole fraction of species Y. The mixture fraction f was derived by formula 2, where $Z_{H_2,flame}$ is the value calculated at each measurement position and $Z_{H_2,fuel}$ is the value calculated from the original fuel composition.

$$Z_{H_2} = \mu_{H,CH_4} \times X_{CH_4} + \mu_{H,H_2O} \times X_{H_2O} + \mu_{H,H_2} \times X_{H_2} \tag{1}$$

$$f = \frac{Z_{H_2,flame}}{Z_{H_2,fuel}} \tag{2}$$

A calibration was used to calculate the species concentration from the measured Raman signals. The temperature was calculated using the ideal gas law. The calibration accounted for the temperature and species concentration dependant Raman scattering signal intensity, as well as for the spectral signal overlap between species. The determination of this calibration was performed by measuring Raman signal from reference gases and flames. The reference gas measurements used were air, CO_2, CO, CH_4 and H_2. The reference gases were preheated to varying temperatures up to 800 K. Hence providing temperature dependence up to 800 K. Methane/air flames varying in equivalence ratio between 0.8-1.4 with temperatures from 1500 K to 2100 K provide the higher temperature range coefficients. These coefficients were used to fit temperature dependant curves. To verify the accuracy of the calibration curves, re-calculation of calibration flame temperatures and species mole fractions were carried out to compare with equilibrium composition and CARS temperature measurements. The accuracy of the calibration

was estimated by calculating the RMS of the percentage difference to actual values for methane/air flames. The accuracy for individual species was 3.9 % for CO_2, 2 % for H_2O, 48 % for CO, 7.37 % for O_2 and 6.8 % for temperature. In order to take into account daily variations in signal intensity due to change in window transmittance air measurements were performed before and after actual flame measurement. A scaling factor was calculated by taking ratio of the respective day reference measurement to laser intensity normalised calibration air reference measurement.

3. Results and Discussion

The stability of swirl stabilized oxyfuel/CH_4 flames was studied for O_2 mole fractions of 20 % - 40 %, equivalence ratios of $\phi = 0.5$ - 1 and thermal powers of 10 kW to 30 kW. However, attempts of operating the burner with $\leq$22 % O_2 were unsuccessful even with conditions of $\phi = 1.0$ at 20 kW and 30 kW resulting in unstable operation and blow out.

Figure 2 shows the range of stable flame operation for different oxidiser compositions and thermal powers versus the Reynolds number. The Reynolds number is calculated using the minimum effective flow cross section of the burner outer co-swirl nozzle (25 mm) with flow rate calculated for standard temperature and pressure. The viscosity of the mixture is calculated using Wilke formulation [12]. The plot shows two sets of iso-power lines, one from 12000<Re<19000 representing 10-20 kW and the second from 19000<Re<28000 for 15-30 kW. Each of the curves in 12000<Re<19000 range starting from the left represents equivalence ratios of 0.49, 0.54, 0.71 and 1. Similarly for 19000<Re<28000 the equivalence ratios are 0.51, 0.71

and 1. It can be seen that as the fraction of O_2 in the oxidiser is reduced by increasing the amount of CO_2, the Reynolds number increases considerably for the same power. This is mainly due to the increased CO_2 content for the same equivalence ratio. The plot indicates that as the O_2 content in the oxidiser is increased the flame can be operated stably for much leaner conditions. This can be attributed to two effects: the flame speed and/or the Reynolds number. In oxyfuel combustion the O_2 fraction of the oxidiser can be seen as an additional variable influencing the combustion behaviour. In fact, the O_2 concentration has a large effect on the flame speed. Measurements of the laminar flame speed, which were carried out as part of this project show, that the flame speed at 6 bar rises by a factor of 2.4 when the O_2 fraction is increased from 30 % to 40 % [13]. Only for O_2 concentrations around 40 % the laminar flame speed is comparable with the flame speed of a laminar CH_4/air flame ($\approx$ 50 cm/s at 6 bar and 473 K preheat temperature). This behaviour is similar also for measurements at 3 bar and 10 bar. Unfortunately no experimental results exist for atmospheric pressure, but it can be expected that the effect at atmospheric pressure is similar to that for pressurized cases. A change of the O_2 concentration is thus expected to have a major effect on the flame stability. The oxidiser composition also influences the flow field. For example, compared to 38 % O_2 oxidiser the 26 % O_2 oxidiser leads to a 40 % increase in Reynolds number for the same equivalence ratio at a power of 20 kW. This effect is described in detail below. The higher flame speed and lower Reynolds number hence assist flame stabilisation and lean operation at higher O_2 levels. The stabilisation behaviour does not change significantly with power, the flames at higher Reynolds number

have similar stability limits.

The influence of variations of the oxygen fraction on the flame is further shown in Fig. 3. Averaged OH^*-chemiluminescence images for flames at 21.4 kW thermal power and $\phi = 0.71$ for 26 %, 30 %, 34 % and 38 % oxygen (left to right) are shown. The displayed images cover a field of view of -42.5 mm $\leq$ r $\leq$ 42.5 mm and 0 mm $\leq$ h $\leq$ 110 mm, where r is the radial position relating to the burner axis, and h is the height above the burner. The images are the ensemble average of 200 short exposures with background correction and normalization applied, so that intensities are comparable between the images. Because of the rotational symmetry of the flame, the 2D images of the integrated signal could be deconvolved by a three point-Abel inversion to derive a section of the symmetry plane through the centre of the flame [14]. None of the flames investigated burned directly at the fuel nozzle; they were thus lifted and partially premixed before ignition. Starting at the left, the OH^*-chemiluminescence intensity for the 26 % O_2 flame is relatively low. The flame zone is distributed almost over the whole combustion chamber, except along the inflow of fresh gas. There is combustion present even in the outer recirculation zone. While increasing the oxygen fraction the flame zone moves upstream towards the burner plate. At 30 % O_2, the flame shape resembles those from stably burning CH_4/air flames in the same combustor. The flames with 34 % and 38 % O_2 exhibited periodic thermo-acoustic pulsations. While non-pulsating flames typically have a conical shape, the flames became flatter with the onset of pulsations. This behaviour was already observed in CH_4/air flames investigated previously in this burner [9]. For CH_4/air as well as for CH_4/oxyfuel, the flames were

subject to thermo-acoustic instabilities over a substantial range of operating conditions. The adiabatic flame temperatures with increasing O_2 content of the flames are 1671 K, 1856 K, 2004 K and 2140 K respectively (flame temperatures calculated with CANTERA). Higher flame temperatures increase, of course, the reactivity leading to higher laminar flame speeds and shorter ignition delay times. This change in chemical reaction rates along with the reduced Reynolds numbers are expected to be main causes for the change of the flame structure.

The results from the laser Raman scattering experiments allow for a more quantitative view into the flame. In the following, results from a flame with P_{th}=22.7 kW, ϕ =0.76, 30 % O_2 are discussed which is very close to the flame in Fig. 3(b). Figure 4 shows radial profiles of the temperature from this flame at different heights, ensemble averaged over 300 laser shots at each measuring location. Near the nozzle, at h=5 and 10 mm, the temperature in the inlet region (r$\approx$ 5-15 mm) is close to room temperature. The scatter plot of temperature and mixture fraction from this region, displayed in Fig. 5(a), yields a more detailed view of the thermo-chemical state of the flame. Here, each symbol represents the result from a single shot measurement at h=10 mm, r=10 mm and the dashed line shows the result from an adiabatic equilibrium calculation. The vertical line indicates the global mixture fraction deduced from the mass flow rates. All four measurement positions of Fig. 5 are marked in Fig. 3(b) by crosses. There is a large scatter in mixture fraction reaching from f=0 (pure oxidiser) to about f=0.15 (corresponding to ϕ =2.96) that reflects the degree of unmixedness in this partially premixed flame. Most of the samples exhibit temperatures around 300 K, i.e., they have not reacted yet.

The samples with increased temperature represent mixtures of fresh gas with some admixtures of exhaust gas from the recirculation zones. Going back to the radial profiles of Fig.4, one can see an increase in temperature from the inflow towards the flame axis. Along the axis, the temperature gradually increases from T=800 K at h=5 mm to T=1900 K at h=60 mm. From velocity measurements in CH_4/air flames performed previously in this burner it can be assumed that this region lies within the IRZ [9]. The scatter plot from h=10 mm, r=0 mm, displayed in Fig. 5(b), shows that the mixtures are relatively fuel rich with a large variation in temperature. The samples with high temperatures (T≈1700 K) are completely reacted and an inspection of the composition reveals that there is no CH_4 present, but small amounts of O_2. The high chemiluminescence intensity observed in this region (see Fig. 3(b)) suggests that these gas mixtures have just reacted. Alternatively, they could have been convected as burned gas from further downstream within the IRZ. The samples with intermediate temperature contain CH_4 and O_2 and probably represent mixtures of burned and unburned gas which has not reacted yet due to ignition delay. The radial temperature profiles in Fig. 4 show a rather flat profile with T≈1400 K at h=5 mm and 10 mm for r>20 mm (Raman measurements could be performed up to r=32.5 mm; the remaining 10 mm to the combustor wall were not accessible due to restrictions of the optical arrangement). This region is supposed to belong to the ORZ. A scatter plot from this region (Fig. 5(c)) exhibits a relatively homogeneous gas mixture close to the global mixture fraction, and an inspection of the molecular composition confirms that it is burned gas. The temperature is, however, approximately 300 K below the adiabatic temperature. This tem-

perature loss might be caused, to some extent, by thermal radiation and certainly to heat loss at the combustor wall and burner plate. Similar effects have been observed before in CH_4/air flames [10] and are typical for samples from the ORZ. The radial temperature profiles in Fig. 4 further show that the temperature level increases with height, as expected, due to reaction progress and reaches the final state at h=60 mm. It is, however, interesting to note that the reaction progress is typically not characterized by one step from unburned to burned mixtures, but rather through intermediate states. This is illustrated in the scatter plot from h=35 mm, r=23 mm, in Fig. 5(d). The samples exhibit temperatures between T=500 K and T=2100 K and almost the complete range of reaction progress from non-reacted to completely reacted. Again, the intermediate temperatures are most likely interpreted as mixtures of burned and unburned gas which have not fully reacted yet due to ignition delay.

A qualitative comparison of these results with CH_4/air flames from previous studies [9, 10] reveals some differences. The temperature level, and thus the reaction progress, in the central region close to the nozzle is smaller in this flame. This is probably due to a different extension of the IRZ. Here, velocity measurements that have not yet been performed could certainly yield more information. Further, the temperature loss in the ORZ is more pronounced in this flame. This might be caused by a larger contribution of thermal radiation of CO_2 in comparison to N_2 and also by a higher heat transfer rate to the wall of CO_2 compared to N_2.

With regard to gas turbine conditions the flame temperature plays an important role. Higher temperature implies higher efficiency of the turbine.

This is manly limited by the material used at the turbine inlet, and for today's gas turbines limited to ≈1600 K. For oxyfuel flames the adiabatic flame temperature at 21 % oxygen is significantly lower compared to CH_4 /air flames at the same stoichiometry. Comparable flame temperatures are reached for an oxygen fraction of 30 %. Because of the high cost of air separation and to have less oxygen diluting the flue gas, it is aspired to burn oxyfuel flames with almost no oxygen in excess near $\phi = 1.0$. For those conditions the adiabatic flame temperature for an oxyfuel flame with 30 % oxygen is 2160 K, much to high for a turbine. To reach acceptable temperatures the oxygen level would have to be lowered to 18 %, which corresponds to an adiabatic flame temperature of 1600 K. As stated above, such a low oxygen concentration would cause a very low laminar flame speed. The results of the measurement show, that even for 30 % O_2 the flame is less stable than a methane/air flame in this burner. For lower O_2 concentrations a stable operation with this kind of burner is not possible. The results from the atmospheric measurements imply, that oxyfuel combustion under technical relevant conditions in a gas turbine burner, which was optimized for CH_4/air combustion, might not be possible. Other burner configurations, which take into account the low flame speed, could improve the flame stabilisation for such cases. But the combustion behaviour of the oxyfuel flames can change under pressurized conditions. Therefore pressurized experiments will be carried out in 2010, in the framework of the BIGCO2 project.

4. Summary and Conclusions

The combustion behaviour of partially premixed CH_4/oxyfuel flames in a swirl stabilized burner for O_2 fractions of 20 % - 40 %, an equivalence ratio of ϕ =0.5 - 1, and thermal powers of P_{th} =10 kW to 30 kW was characterized by using OH^*-chemiluminescence to monitor the flame structure and flame stability. Flames could be stabilized over a wide parameter range. The O_2 fraction had a strong influence on the flame shape, whereas changes in equivalence ratio only had marginal effects. At some of the operating conditions, the flames exhibited periodic thermo-acoustic instabilities. For a flame with P_{th} =22.7 kW, ϕ =0.76 and O_2 concentration of 30 %, single-shot laser Raman measurements have been performed for the simultaneous determination of the major species concentrations, mixture fraction and temperature. A significant variation in mixture fraction and reaction progress was observed with non-reacted, partially and completely reacted samples.

Compared to CH_4/air flames which have been investigated previously in the same burner, the CH_4/oxyfuel flames studied here showed a different combustion behaviour. For the stabilization of these flames, the O_2 fraction in CO_2 had to be larger than the 21 % in air. The main reasons are obviously the larger heat capacity of CO_2 compared to N_2 that leads to lower combustion temperatures for the same equivalence ratio and the lower laminar flame speed. The Raman measurements revealed a significant difference between the temperature measured in the outer recirculation zone and the adiabatic flame temperature. This temperature loss is probably due to thermal radiation and heat loss to the walls of the combustor. The heat loss was larger than previously observed for CH_4/air flames. There were also indications

that the inner recirculation zone does not extend so far upstream as it was measured for CH_4/air.

5. Acknowledgments

This publication forms a part of the BIGCO2 project, performed under the strategic Norwegian research program Climit. The authors acknowledge the partners: Statoil, GE Global Research, Statkraft, Aker Clean Carbon, Shell, TOTAL, ConocoPhillips, ALSTOM, the Research Council of Norway (178004/I30 and 176059/I30) and Gassnova.

6. References

[1] McKinsey & Company, availible at <http://www.mckinsey.com/-clientservice/ccsi/pdf/CCS_Assessing_ the_Economics.pdf>

[2] H. Jericha, W. Sanz, K. Woisetschläger, M. Fesharaki, CIMAC Conference, Interlaken, Switzerland, 1995.

[3] H. Jericha, W. Sanz, E. Göttlich, F. Neumayer, ASME Turbo Expo (2008) GT2008-50515.

[4] K. Foy, E. Yantovski, Int. J. of Thermodynamics 9 (2) (2006) 37-63.

[5] N. Zhang, N. Lior, Energy 33 (2008) 340-351.

[6] T. C. Williams, C. R. Shaddix, R. W. Schefer, Combust. Sci. and Tech. 180 (2008) 64-88.

[7] J. C. Sautet, L. Salentey, M. Ditaranto, J. M. Samaniego, Combust. Sci and Tech. 166 (2001) 131-150.

[8] M. Ditaranto, J. Hals, Combust. Flame 146 (2006) 493-512.

[9] P. Weigand, W. Meier , X. R. Duan, W. Stricker, M. Aigner, Combust. Flame 144 (2006) 205-224.

[10] W. Meier , X. R. Duan, P. Weigand, Combust. Flame 144 (2006) 225-236.

[11] H. Ax, P. Kutne, W. Meier, K. König, U. Maas, A. Class, M. Aigner, Appl. Phys. B. 94 (2009) 705-714.

[12] J. Warnatz, U. Maas, R.W. Dibble, Combustion, Springer, 2006, p. 64.

[13] J. Herzler, C. Naumann, Proc. Combust. Inst. 33 (2010) submitted.

[14] C.J. Dasch, Appl. Opt. 31 (1992) 1146.

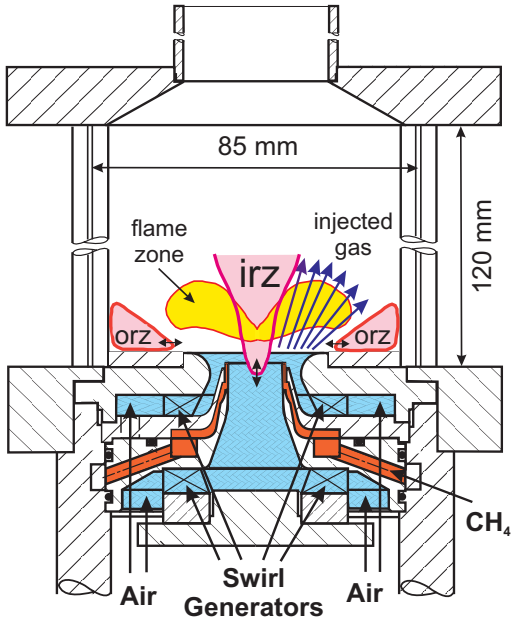

Figure 1: Nozzle and combustion chamber of the DLR burner.

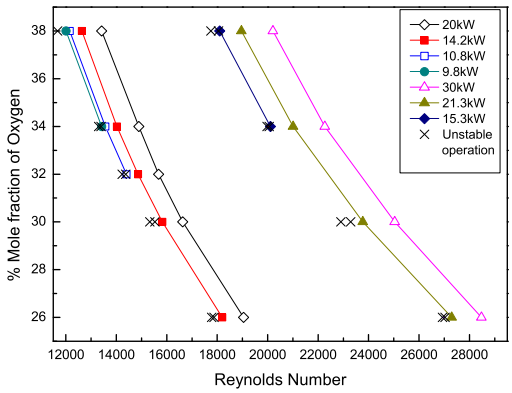

Figure 2: Stable flame operation for different mixtures and power levels.

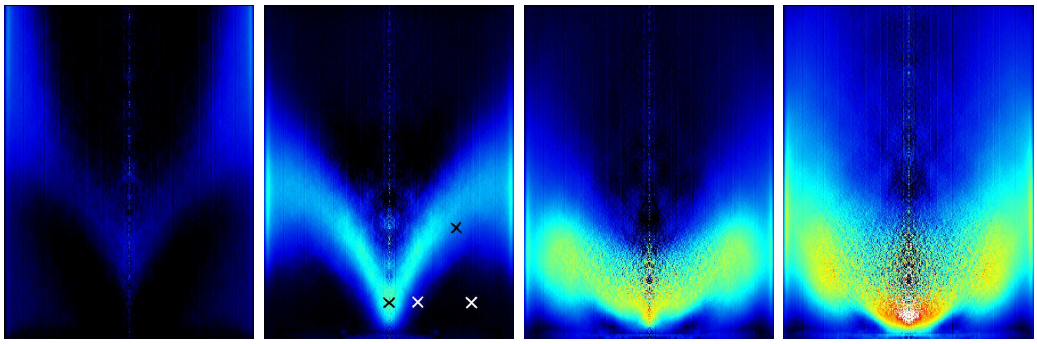

(a) 26 % O_2 (b) 30 % O_2 (c) 34 % O_2 (d) 38 % O_2

Figure 3: Abel-deconvoluted OH^*chemiluminescence images showing average flame structure at power of 21.4 kW and $\phi = 0.71$ for different O_2 mole fractions 3(a) 26 %, 3(b) 30 %, 3(c) 34 %, 3(d) 38 %.

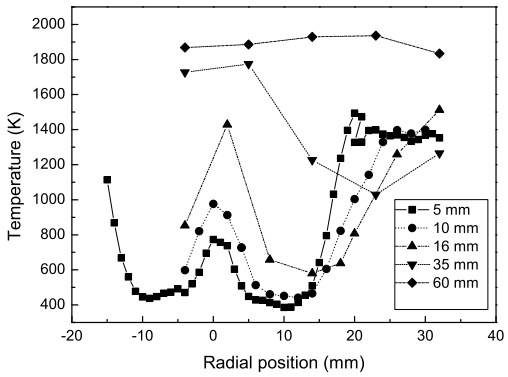

Figure 4: Radial profiles of mean temperature at different heights above the burner for the flame with P_{th}=22.7 kW, ϕ =0.76, 30 % O_2.

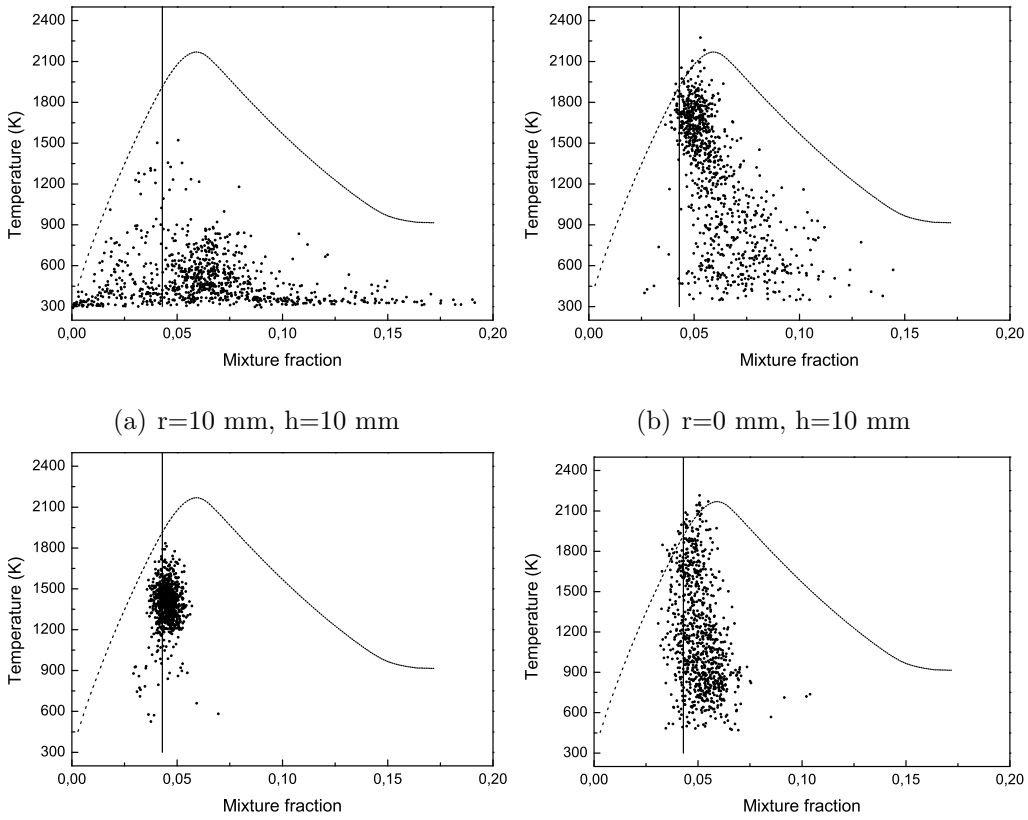

(a) r=10 mm, h=10 mm

(b) r=0 mm, h=10 mm

(c) r=28 mm, h=10 mm

(d) r=23 mm, h=35 mm

Figure 5: Raman scatter plots for a flame with P_{th}=22.7 kW, ϕ =0.76, 30 % O_2, showing the correlation of temperature and mixture fraction at four different positions in the flame. r is the radial position relating to the burner axis, and h is the height above the burner. Dashed line represents results from adiabatic equilibrium calculations and vertical line indicates global mixture fraction.

Figure captions:

Fig. 1. Nozzle and combustion chamber of the DLR burner.

Fig. 2. Stable flame operation for different mixtures and power levels.

Fig. 3. Abel-deconvoluted OH*chemiluminescence images showing average flame structure at power of 21.4 kW and $\phi = 0.71$ for different O_2 mole fractions 3(a) 26 %, 3(b) 30 %, 3(c) 34 %, 3(d) 38 %.

Fig. 4. Radial profiles of mean temperature at different heights above the burner for the flame with P_{th}=22.7 kW, ϕ =0.76, 30 % O_2.

Fig 5. Raman scatter plots for a flame with P_{th}=22.7 kW, ϕ =0.76, 30 % O_2, showing the correlation of temperature and mixture fraction at four different positions in the flame. r is the radial position relating to the burner axis, and h is the height above the burner. Dashed line represents results from adiabatic equilibrium calculations and vertical line indicates global mixture fraction.